Article

Mercator, Fortaleza, v.21,e21019, 2022. ISSN:1984-2201

SENTINEL-1 TIME SERIES ANALYSIS ON CENTRAL AMAZON FLOODS

https://doi.org/10.4215/rm2022.e21019

Ivo Augusto Lopes Magalhães [a]* - Osmar Abílio de Carvalho Junior [b] - Renato Fontes Guimarães [c]
Roberto Arnaldo Trancoso Gomes [d]

(a) PhD in Geography. University of Brasilia, Brasilia (DF), Brazil.
ORCID: https://orcid.org/0000-0003-4136-1972. **LATTES:** http://lattes.cnpq.br/6217252445608239.
(b) PhD in Geology. Professor at University of Brasilia, Brasilia (DF), Brazil.
ORCID: https://orcid.org/0000-0002-0346-1684. **LATTES:** http://lattes.cnpq.br/5572269831914055.
(c) PhD in Geology. Professor at University of Brasilia, Brasilia (DF), Brazil.
ORCID: https://orcid.org/0000-0002-9555-043X. **LATTES:** http://lattes.cnpq.br/7063856452054362.
(d) PhD in Geography. Professor at University of Brasilia, Brasilia (DF), Brazil.
ORCID: https://orcid.org/0000-0003-4724-4064. **LATTES:** http://lattes.cnpq.br/1886939214378140.

Article history:
Received 24 November, 2021
Accepted 08 July, 2022
Published 15 October, 2022

(*) CORRESPONDING AUTHOR
Address: UnB. Departamento de Geografia, GEA, ICC Norte 900, Brasília (DF), Brasil.
Tel: (+55 38) 98831-3917.
E-mail: ivosrmagalhaes@gmail.com

Abstract

This study aimed to analyze the dynamics of the flooded areas of the Sentinel 1-SAR time series in a section of the Central Amazon between September 26, 2016, and February 8, 2020. The total of images was 59 for each polarization. In addition, the study calculated the average ordinary flood line (ALOF) from the heights of the fluviometric rulers between the years 1967 to 2020 and compared it with the values present in the radar time series. The pre-processing of the Sentinel-1 time series in the VV and VH polarizations used the following methodological sequence: Apply Orbit File, Radiometric Calibration (σ0), Range-Doppler Terrain Correction, Speckle Filter, and conversion to decibels (dB). The previous analysis of the adaptive filters showed different results for the two polarizations, obtaining the best result for the VV polarization using the Frost filter with 3x3 and the VH polarization with the Lee filter 3x3. The extraction of water bodies and wetlands used a threshold value, making masks for the entire period. The most considerable extent of the floodable area occurred on June 17, 2019, with 6,611.86 km2, representing 16.42% of the SAR scene in the VH polarization and 6,443.19 km2, representing 16.10% of the SAR scene in the VV polarization. The relationship between the VH and VV wetlands to the ruler's height was satisfactory, with coefficients of determination (R2) of 0.79 in the VH polarization and of 0.64 in the VV polarization and a p-value less than 0.05.

Keywords: Remote sensing; Radar; Mapping of Water Bodies.

Resumo / Resumen

ANÁLISE DA SÉRIE TEMPORAL SENTINEL 1 DE INUNDAÇÕES NA AMAZÔNIA CENTRAL

Este estudo teve como objetivo analisar a dinâmica das áreas alagadas da série temporal Sentinel-1 SAR em um trecho da Amazônia Central no período entre 26 de setembro de 2016 e 8 de fevereiro de 2020. O total de imagens foi de 59 para cada polarização. Além disso, a pesquisa calculou a linha de inundação ordinária média (LMEO) a partir das alturas das réguas fluviométricas entre os anos de 1967 a 2020 e a comparou com os valores presentes na série temporal do radar. O pré-processamento da série temporal Sentinel-1 nas polarizações VV e VH utilizou a seguinte sequência metodológica: correção de órbita, correção radiométrica (σ0), correção do terreno, filtragem do ruído, e conversão dos dados para decibéis (dB). A análise prévia dos filtros adaptativos mostrou resultados diferentes para as duas polarizações, obtendo o melhor resultado para a polarização VV utilizando o filtro Frost com 3x3 e para a polarização VH o filtro Lee 3x3. A extração de corpos d'água e áreas úmidas utilizou um valor limite fazendo máscaras para todo o período. A maior extensão da área inundável foi medida em 17 de junho de 2019, com 6.611,86 km2, representando 16,42% da cena SAR na polarização VH e 6.443,19 km2, representando 16,10% da cena SAR na polarização VV. A relação entre as áreas úmidas VH e VV em relação à altura da régua foi satisfatória, com coeficientes de determinação (R2) de 0,79 na polarização VH e de 0,64 na polarização VV e p-valor menor que 0,05.

Palavras-chave: Sensoriamento Remoto; Radar; Mapeamento de Corpos Hídricos.

ANÁLISIS DE SERIE DE TIEMPO SENTINEL 1 SOBRE INUNDACIONES EN LA AMAZONIA CENTRAL

Este estudio tuvo como objetivo analizar la dinámica de las áreas inundadas de la serie temporal Sentinel-1 SAR en una sección de la Amazonía Central en el período comprendido entre el 26 de septiembre de 2016 y el 8 de febrero de 2020. El total de imágenes fue de 59 para cada polarización. Además, la investigación calculó la línea de inundación ordinaria promedio (LMEO) a partir de las alturas de las reglas fluviométricas entre los años 1967 a 2020 y la comparó con los valores presentes en la serie temporal del radar. El preprocesamiento de la serie temporal Sentinel-1 en las polarizaciones VV y VH utilizó la siguiente secuencia metodológica: corrección de órbita, calibración radiométrica (σ0), corrección del terreno, filtrado de ruido y conversión a decibelios (dB). El análisis previo de los filtros adaptativos mostró resultados diferentes para las dos polarizaciones, obteniendo el mejor resultado para la polarización VV utilizando el filtro Frost con 3x3 y para la polarización VH el filtro Lee 3x3, realizando máscaras para todo el periodo. La mayor extensión del área inundable se midió el 17 de junio de 2019, con 6.611,86 km2, que representa el 16,42 % de la escena SAR en polarización VH y 6.443,19 km2, que representa el 16,10 % de la escena SAR en polarización VV. La relación entre los humedales VH y VV en relación con la altura de la regla fue satisfactoria, con coeficientes de determinación (R2) de 0.79 en la polarización VH y de 0.64 en la polarización VV y p-valor menor a 0.05.

Palabras-clave: Detección remota; Radar; Mapeo de cuerpos de agua.

INTRODUCTION

The most significant extensions of floodable areas in Brazil are in the Pantanal and Amazon biomes. The Amazon River is responsible for approximately 12% of the total wetland area in the Amazon basin, having a wide variety of herbaceous, shrub and arboreal phytophysiognomies, both terrestrial and aquatic (MELACK and HESS, 2010).

In the national territory, the wetlands adjacent to federal rivers are property of the Union. The Federal Constitution of 1988, in its article 20, defines that the Union manages the following areas: public lands not allocated by the Government, lakes, rivers and any water currents in lands under its domain; river and lake islands in frontier areas with other countries; the sea beaches; oceanic and coastal islands; the territorial sea; the navy lands; mineral resources; archaeological and prehistoric sites; indigenous lands; among others (BRASIL, 1988).

Decree-Law nº 9,760, of September 5, 1946, defines Marginal Lands as areas bathed by navigable waters, outside the reach of the tides, with fifteen meters measured horizontally towards land counted from the Average Line of Ordinary Floods (ALOF). The definition of Marginal Lands considers understanding the flood pulse dynamics of the federal rivers.

The ALOF calculation uses data from historical series of fluviometric stations considering the maximum annual average of the flood quota for at least 20 years. Another critical data is the geodesic landmark closest to the demarcation section to carry out the topographic levelling with transposition of the altimetric elevation between the geodetic landmark and the relative height of the fluviometric station, thus obtaining the topographic height of the ALOF (SPU, 2001).

The extensive rivers and uninhabited areas in the Amazon biome make the in-situ information acquisition quite expensive due to the demand for planning, equipment, transport, and human resources. Thus, remote sensing and geoprocessing techniques are viable alternatives for obtaining and collecting information about water bodies.

Optical satellite images in the Amazon region have limitations due to intense interference from cloud coverage throughout the year (FORKUOR et al., 2014). Therefore, radar systems are the most suitable for monitoring this region by pass through clouds and nebulosity. A SAR system uses sophisticated signal processing to synthesize an antenna more extensive than its actual physical size. The Sentinel-1 SAR satellite belonging to the European Space Agency (ESA) mission was launched in 2014, with a microwave sensor operating in the C-band in single (HH or VV) or dual (HH/HV or VV/VH) polarization modes and high spatial and temporal resolution.

However, the main interference factor associated with the interpretation of RADAR image is the presence of speckle noise (TELLO, LOPEZ-MARTINEZ and MALLORQUI, 2006; CHANG et al., 2007; SANTOSO et al., 2016). The speckle noise generates a granular appearance in the image, composed of sudden changes in the grey level in spatially close pixels (FURTADO et al., 2016). Therefore, this noise degrades the quality of the images, interfering in all stages of detection of dark targets, requiring the use of processing in multiple views (multi-look) or the application of filters for its smoothing (DONG, MILNE, and FORSTER, 2001 and FURTADO et al., 2016).

The present research aims to measure the floodable areas and the ALOF through fluviometric data (1967-2020) and time series of Sentinel 1-SAR images (2016-2020) in dual-polarization VH and VV in a highly floodable stretch of Amazon.

MATERIALS AND METHODS

STUDY AREA

The study area is located between the municipalities of Urucará and Parintins east of Manaus in the state of Amazonas, comprising the Amazon River in the quadrant with the geographic coordinates 2º 32' 11"S 57º 45' 38"W and 2º 37' 42"S 56º 44' 11"W (Figure 1). The climate is "Am" in the Köppen classification, with an annual rainfall of 1,355 to 2,839 mm. The flood period begins in May and extends until mid-July, followed by the dry period between September and November (RAMALHO et al., 2009).

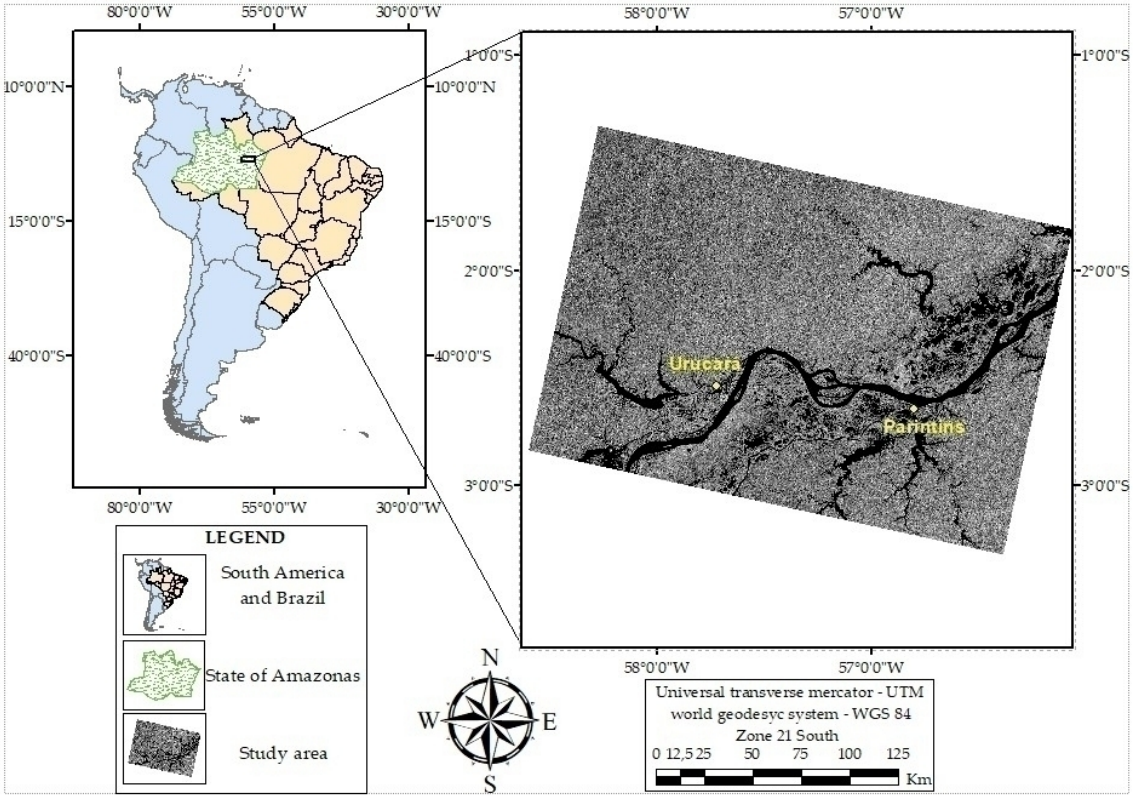

Figure 1 - Geographic location of the study area in Central Amazon.

SENTINEL-1 IMAGES AND PRE-PROCESSING

Sentinel-1 (SAR) images are freely available on the European Space Agency (ESA) website (https://scihub.copernicus.eu/dhus/#/home), with different characteristics (Table 1). The present study acquired 59 Sentinel-1 satellite images in the VH and VV polarization in the Central Amazon region in the annual period between September 26, 2016, and February 8, 2020. The images correspond to the Interferometric Wide Swath (IWS) mode, descending with level 1 ground range detected (GRD). The pre-processing used the Sentinel Application Platform (SNAP) software version 7.0.0, considering the following methodological sequence: Appy Orbit File, Radiometric Calibrate (σ0), Geometric Correction (Range-Doppler Terrain Correction), Speckle Filter and conversion of data from linear to decibels (dB).

Modes	Incidence angle	Spatial Resolution	Ground range coverage	Polarization
SM	20° - 45°	5 × 5 m	80 km	HH/HV, VV/VH, HH, VV
IW	29° - 46°	5 × 20 m	250 km	HH/HV, VV/VH, HH, VV
EW	19° - 47°	20 × 40 m	400 km	HH/HV, VV/VH, HH, VV
WV	22° - 35°	5 × 5 m	20 × 20 km	HH, VV
	35° - 38°			

Table 1 - Parameters of the Sentinel-1 mission acquisition modes. Source: ESA (2017).

The software used in the geoprocessing and data validation phases were Envi 5.5 and ArcGIS 10.6. The temporal extraction of the water bodies and floodable areas used the masking technique in the temporal cube of the SAR images from the definition of a threshold value using the Envi 5.5 program. Subsequently, we convert the masks into vectors to measure the flooded areas and define the ALOF for

the region under study.

DATA FILTERING

Speck noise caused by additive or destructive interference from the radar return signal to each cell impairs the visual interpretation of images (Lee and Pottier, 2009). The selection of the best filter for each polarization considered seven filtering methods (Frost; Gamma Map; Lee Enhanced; Lee; IDAM 1, 2, and 3; median; and Boxcar) in three window dimensions (3x3, 7x7, and 11x11). The analysis used 40 samples evenly distributed throughout the reference image with a size of 5,000 km2. Metrics analyzed were: Mean Square Error (MSE), Mean Absolute Error (MAE), Signal-to-Noise Ratio (SNR), Peak Signal to Noise Ratio (PSNR), Edge Preservation Index (EPI), Contrast Distortion (DCON), and Equivalent Number of Looks (NEL).

TEMPORAL CUBE ELABORATION

The temporal cube assembly considered the 59 SAR images in the VH and VV polarizations from 09/26/2016 to 02/08/2020. The temporal cube displays the geographic coordinates on the “x (lines)” and “y (columns)” axes and the temporal trajectory on the “z” axis with the sequence of days in ascending order (CARVALHO JUNIOR et al., 2008). Therefore, z attribute of the temporal cube describes the presence of floodable areas in the two polarizations, VH and VV.

WIND FIELDS

Wind speed influences the SAR backscatter values in the Amazon River, Lago Grande and Lago Moratinga in the VH and VV polarizations. The wind speed data (meters per second) used comes from the Meteorological Data Bank System for Teaching and Research (BDMEP) and the National Institute of Meteorology (INMET) (Table 2). The research used 14 rainfall stations located in the Central Amazon and three stations located in the state of Pará to eliminate the edge effect in the interpolation procedure (GARDIMAN JUNIOR et al., 2012). The wind speed interpolation used the averages of the 17 stations, comprising the same days of the SAR images between 09/01/2016 and 02/08/2020 (Figure 2). According to Gardiman Junior et al. (2012), the regularized spline interpolation technique maintains the same sample data value at the station local, in addition to being a deterministic, exact, and non-convex method.

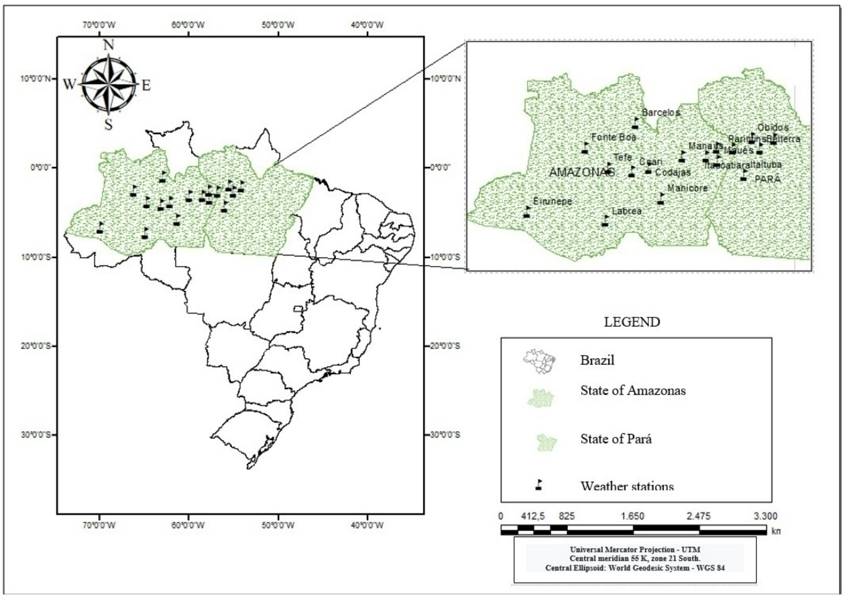

Figure 2 - Map of meteorological stations used for interpolation of wind fields in Central Amazon, state of Pará.

Station	County and state	Latitude	Longitude	Average Wind speed (mps)
82240	Parintins, AM	-2,630	-56,730	1,03
A1222	Maués, AM	-3,399	-57,673	1,14
82317	Tefé, AM	-3,830	-64,700	0,52
82425	Coari, AM	-4,080	-63,130	1,15
82331	Manaus, AM	-3,110	-59,950	0,91
82336	Itacoatiara, AM	-3,130	-58,430	1,13
82113	Barcelos, AM	-0,960	-62,910	0,99
82326	Cadajás, AM	-3,830	-62,080	1,93
82533	Manicoré, AM	-5,8100	-61,300	0,68
82445	Itaituba, PA	-4,2800	-56,000	0,94
82178	Obidos, AM	-1,910	-55,510	1,66
82246	Belterra, PA	-2,630	-54,950	0,94
82181	Monte Alegre, PA	-2,000	-54,080	2,99
82723	Labrea, AM	-7,2500	-64,830	1,9
82212	Fonte Boa, AM	-2,530	-66,160	1,1
82610	Eirunepe, AM	-6,660	-69,860	0,04
A124	Urucará, AM	-2,534	-57,758	1,12

Table 2 - Nomenclature of meteorological stations and wind speed data. Source: INMET, (2020).

CALCULATION OF AVERAGE LINE OF ORDINARY FLOODS - ALOF

The ALOF calculation used the fluviometric data from the historical series (1967-2020) of the Amazon River in the municipality of Parintins, obtained through the hidroweb site (http://www.snirh.gov.br/hidroweb/) of the National Water Agency (ANA). The technical procedures followed the Normative Guidance for the Demarcation of Marginal Lands (SPU, 2001). The ALOF estimate used a historical series of 65 years, referring to the station code ANA 16350002 and considering a minimum return period of 3 years and a maximum of 20 years. By averaging the sum of the highest monthly readings of the river ruler, obtaining an ALOF in centimetres based on the local ruler for the Amazon River in the region of Parintins, AM. This data must be further calculated to obtain its topographic altitude. The day closest to the ALOF (at age 65) in the SAR short time series (4 years) corresponds to the largest inundated area.

STATISTICAL ANALYSIS OF TIME SERIES

Linear regression analysis and Pearson's correlation compared the following data: values measured between the VH and VV polarizations, the relationship between the inundation area obtained by the SAR time series with the fluviometric ruler quotas and accumulated precipitation for each month in Parintins, AM Meteorological Station. This analysis allows estimating a function between the flooded area and the data measured in the field. The methodological flowchart summarizes the steps developed in this study (Figure 3).

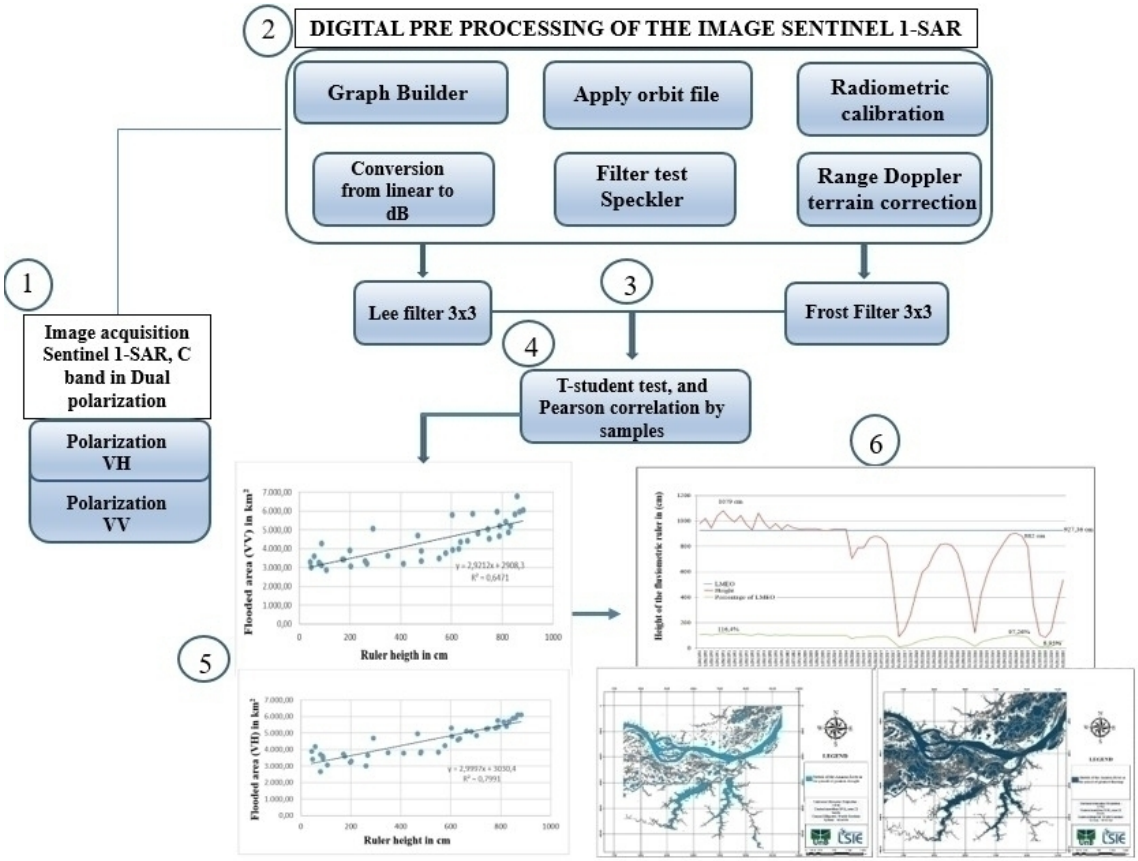

Figure 3 - Methodological flowchart of the steps performed in the flood analysis in the central stretch of the Amazon River.

RESULTS AND DISCUSSION

ANALYSIS OF IMAGE DENOISING TECHNIQUES

Speckle noise is pervasive throughout the SAR scene, with high interference in water bodies. Visual analysis of SAR images demonstrates that spatial filtering significantly minimizes the noise fraction, increasing the clarity of the Amazon River, water bodies and vegetation at polarizations. Tables 3 and 4 list the statistical values of the different filtering techniques for SAR images in VH and VV polarizations. The best results were different between the two polarizations. In the VH polarization, the Lee 3x3 filter showed the best results in noise reduction with the lowest MSE (1.88) and MAE (1.638), as well as the highest values of PSNR (13.35) and SNR (10.27). Most filters showed approximate results, but the Frost 3x3 filter showed the most significant discrepancy between filtering techniques in VH polarization with high MSE (8.95), MAE (6.28), and contrast distortion. In the VV polarization, the Frost filter with 3x3 obtained the best performance with low values for MSE (1.2), MAE (628), and contrast distortion window.

VV Filters	MSE	MAE	SNR	PSNR	CoC	DCON	NEL
Frost 3x3	**1,2**	**6,26**	**13,54**	**12,51**	**0,91**	6,59	12,09
Frost 7x7	3,4	6,28	8,97	12,09	0,75	6,59	17,67
Frost 11x11	4,5	6,27	8,11	11,97	0,64	6,59	21,78
G M 3x3	2,1	6,28	11,58	12,29	0,85	6,59	11,65
G M 7x7	3,9	6,27	8,92	12,03	0,7	6,6	18,38
G M 11x11	4,4	6,27	8,06	11,98	0,65	6,59	23,48
Lee Enhanced	4,1	6,29	7,86	12,01	0,7	**6,58**	14,02
Lee 3x3	3,7	6,27	9,44	12,06	0,74	6,6	11,559
Lee 7x7	4,9	6,27	7,78	11,93	0,61	6,59	18,17
Lee 11x11	5	6,27	7,73	11,92	0,6	6,6	21,23
IDAM 1	3,5	6,28	8,7	12,08	0,75	6,59	19,74
IDAM 2	4	6,28	8,33	12,02	0,7	6,59	20,13
IDAM 3	6,4	6,29	5,77	11,82	0,5	**6,58**	15,45
Mediana 3x3	2,5	6,29	3,76	11,22	0,22	**6,58**	10,49
Mediana 7x7	4,7	6,28	7,43	11,95	0,63	6,59	19,81
Mediana 11x11	5	6,28	6,99	11,92	0,6	**6,58**	25,58
Boxcar 3x3	3	6,28	8,34	11,15	0,68	6,59	18,74
Boxcar 7x7	2,9	6,27	7,14	11,16	0,55	6,59	24,62
Boxcar 11x11	2,9	6,27	7,55	11,15	0,57	6,6	**39,78**

Table 3 - Values of the metric indices for the filtering techniques in the VH polarization.

VV Filters	MSE	MAE	SNR	PSNR	CoC	DCON	NEL
Frost 3x3	**1,2**	**6,26**	**13,54**	**12,51**	**0,91**	6,59	12,09
Frost 7x7	3,4	6,28	8,97	12,09	0,75	6,59	17,67
Frost 11x11	4,5	6,27	8,11	11,97	0,64	6,59	21,78
G M 3x3	2,1	6,28	11,58	12,29	0,85	6,59	11,65
G M 7x7	3,9	6,27	8,92	12,03	0,7	6,6	18,38
G M 11x11	4,4	6,27	8,06	11,98	0,65	6,59	23,48
Lee Enhanced	4,1	6,29	7,86	12,01	0,7	**6,58**	14,02
Lee 3x3	3,7	6,27	9,44	12,06	0,74	6,6	11,559
Lee 7x7	4,9	6,27	7,78	11,93	0,61	6,59	18,17
Lee 11x11	5	6,27	7,73	11,92	0,6	6,6	21,23
IDAM 1	3,5	6,28	8,7	12,08	0,75	6,59	19,74
IDAM 2	4	6,28	8,33	12,02	0,7	6,59	20,13
IDAM 3	6,4	6,29	5,77	11,82	0,5	**6,58**	15,45
Mediana 3x3	2,5	6,29	3,76	11,22	0,22	**6,58**	10,49
Mediana 7x7	4,7	6,28	7,43	11,95	0,63	6,59	19,81
Mediana 11x11	5	6,28	6,99	11,92	0,6	**6,58**	25,58
Boxcar 3x3	3	6,28	8,34	11,15	0,68	6,59	18,74
Boxcar 7x7	2,9	6,27	7,14	11,16	0,55	6,59	24,62
Boxcar 11x11	2,9	6,27	7,55	11,15	0,57	6,6	**39,78**

Table 4 - Values of the metric indices for the filtering techniques in the VV polarization.

Therefore, spatial filtering through Lee 3x3 filters in VH polarization and Frost 3x3 in VV

polarization significantly minimized the noise fraction (Figure 4).

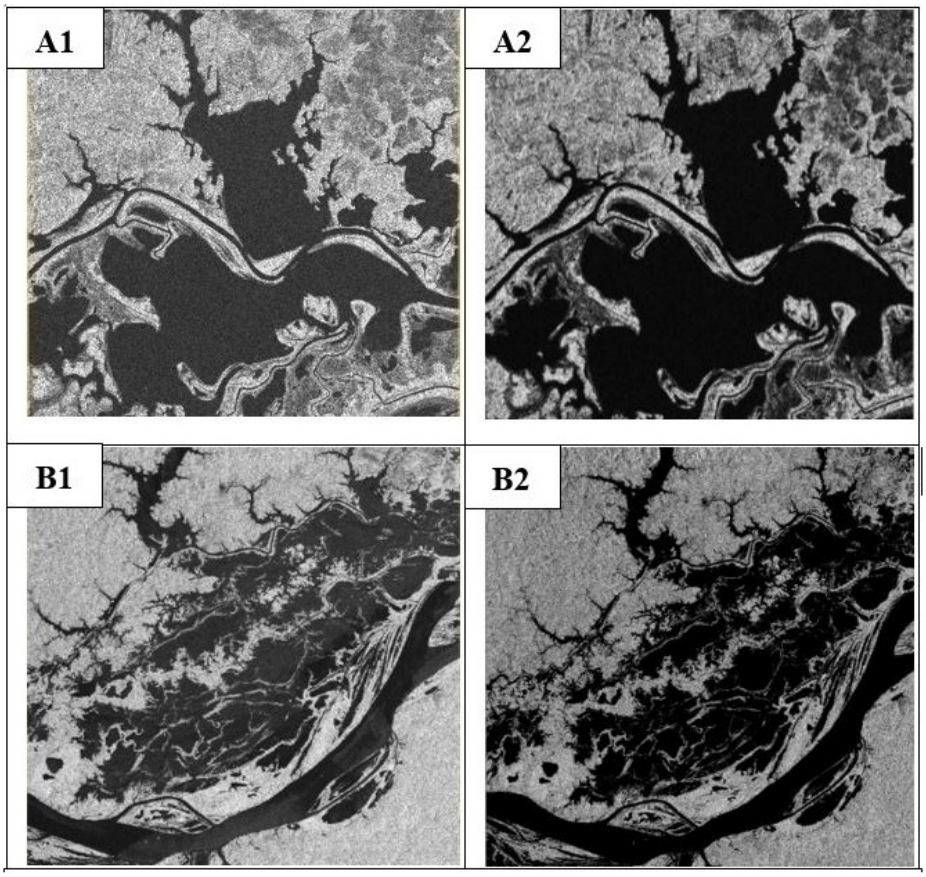

Figure 4 –Sentinel-1 image of water bodies in VH polarization (A1) and filtered by Lee 3x3 (A2), and in VV polarization (B1) and filtered by Frost 3x3.

TEMPORAL CUBE ANALYSIS

The temporal cube allows the analysis of the seasonal dynamics of the flooded areas, with a higher volume of water bodies in May, June, and July and a lower volume in November, December, and January. Figure 5 demonstrates that the VV and VH polarizations do not present a significant visual difference for the water bodies.

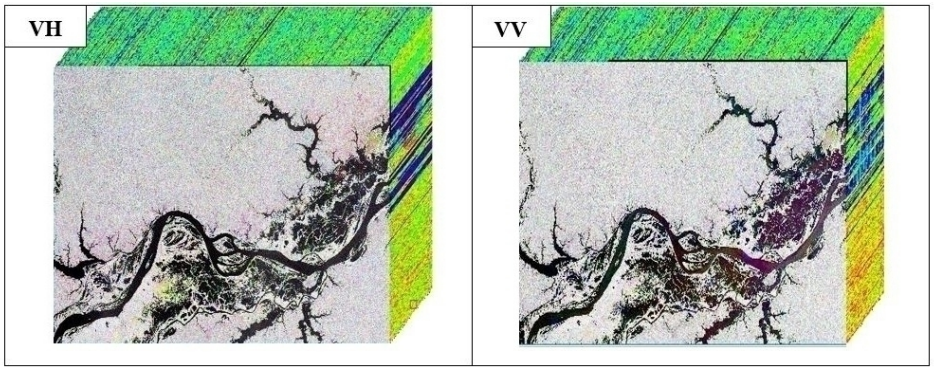

Figure 5 - Temporal cube composed of 59 Sentinel-1 images in the VH and VV polarizations between 09/26/2016 and 02/08/2020.

However, the inability of the C-band to penetrate treetops (approximately 5 cm) makes it

challenging to measure wetlands reliably over forest cover. Marques et al. (2017) analysed wetlands using a temporal cube of PALSAR/ALOS-2 images on Bananal Island, the middle section of the Araguaia River in the state of Tocantins. These authors concluded that the variation of the inundation area was 10% between the images with the lowest and highest flood quotas.

Ferreira (2018) used a temporal cube of 29 Sentinel-1 images with the Random Forest machine learning method and the threshold value in SAR images to identify wetlands in southern Roraima state throughout 2017. The results demonstrated the behaviour typical of flooded areas on the banks of rivers and features adjacent to the Rio Branco. In July, the flood's peak covered more than 72,000 ha of the study area, and the drought's peak in December covered more than 37,000 ha.

CHARACTERIZATION OF THE SAR BACKSCATTER OF WATER BODIES

The temporal analysis of the SAR backscatter values allows characterizing the Amazon River, Grande Lake and Moratinga Lake with values between (-21.49 to -25.78 dB, -22.52 to -28.2 dB and -21, 98 to -27.69 dB in VH polarization and -13.34 to -23.27 dB, -18.14 to -24.57 dB and -17.36 to -26.44 dB) for VV polarization (Figure 6).

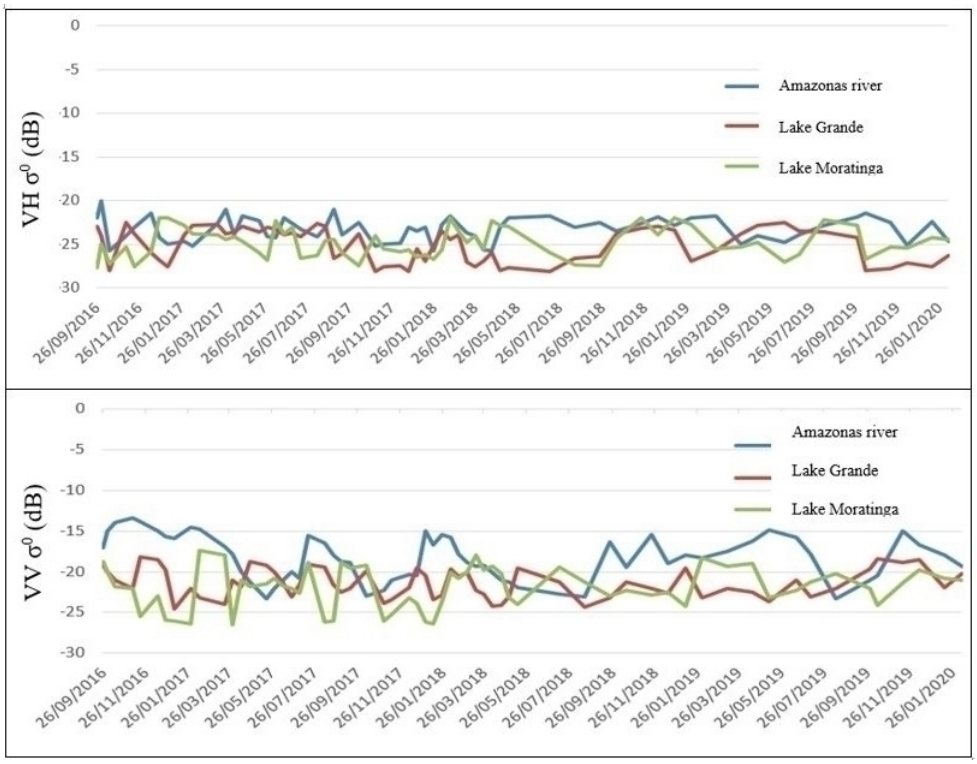

Figure 6 - Graph of SAR backscatter values in the VH and VV polarizations in the Amazon River, Lake Moratinga and Lake Grande in the Central Amazon from 09/26/2016 to 02/08/2020.

The water bodies in the region presented different threshold values in the two polarizations, with an average value of -19 dB in the VH polarization and -14 dB in the VV polarization. Other studies in open water obtained similar values (ARNESEN, 2012; FERREIRA, 2018; FROTA, 2019). However, the Amazon River backscatter values were higher in both polarizations than in Grande and Moratinga Lakes, which presented similar values in both polarizations (VH and VV). The cause of this variation may be due to the following factors: (a) interference of wind fields with speed varying between 1.2 to 1.4 MPS over the Amazon River, superior to the other two lakes (1 to 1.2 MPS), and (b) action of the water current containing more significant ripples in the river and inferring a greater SAR backscatter response (Figure 7). Marinho et al. (2012) corroborate this study by measuring similar backscatter values of water bodies and wetlands in Vale do Itajaí, Santa Catarina state, in SAR images from the

ALOS-PALSAR Sensor.

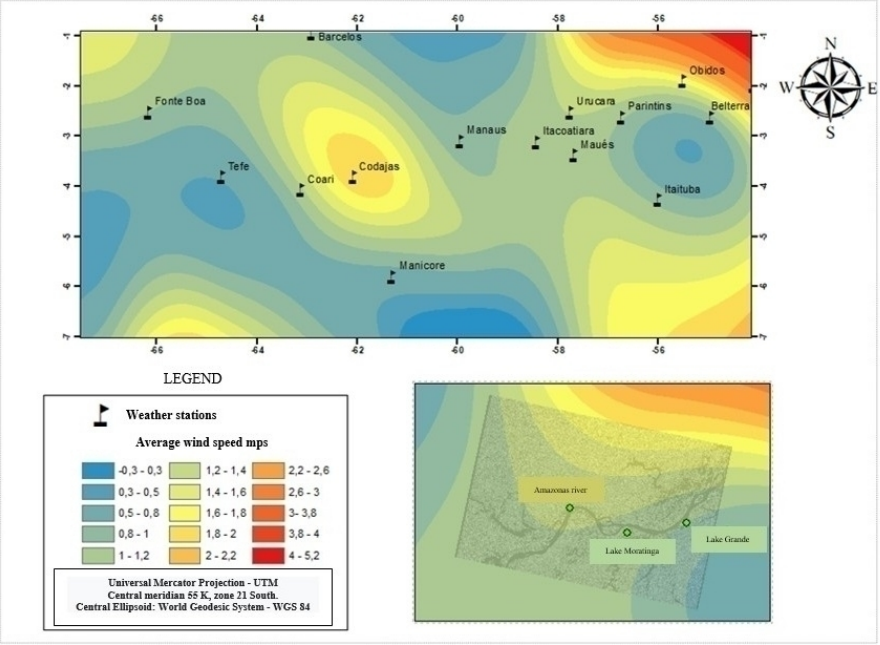

Figure 7 - Map of the average wind speed from 09/01/2016 to 02/08/2020 for Central Amazon.

ANALYSIS OF RAINFALL DYNAMICS AND FLOOD PULSE

The time series of rainfall between 2000 and 2020 in the study area showed that the highest monthly averages occurred in February (313 mm/year), March (378 mm/year) and April (342 mm/year). The lowest values of the monthly averages of precipitation occurred in September (47 mm/year), October (78 mm/year) and November (89 mm/year) (Figure 8). The results corroborate other studies (JUNK, 1997; ARNESEN, 2012) that show a flood pulse of annual monomodal behaviour in the Amazon River and its tributaries, a predictable occurrence throughout the year with the flood period between May and July and the drought between October and December.

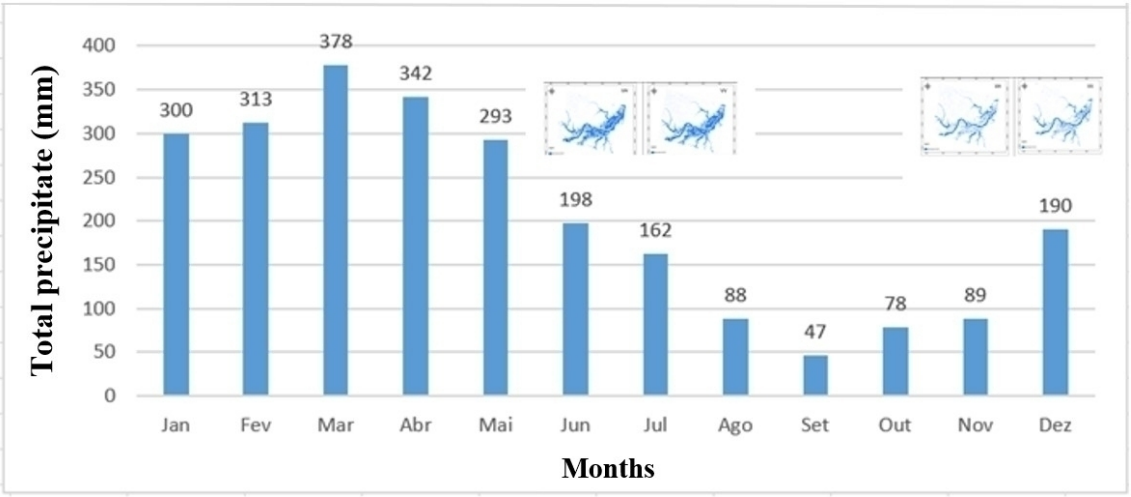

Figure 8 - Rainfall values at Parintins station (AM), highlighting the largest and smallest flooded area within the Sentinel - 1 time-series between 2000 and 2020.

The largest floodable area ensued on June 17, 2019, with 6,611.86 km² representing 16.42% of the VH scene and 6,443.19 km² representing 16.10% of the VV scene. The smallest flooded area occurred on December 25, 2016, with 3,059.75 km² representing 7.64% of the VH scene and 2,868.59 km² representing 7.17% of the VV scene. The SAR images in the two polarizations (VH and VV) show a similarity between the flooded areas in the rainy and dry periods being the differences practically imperceptible (Figure 9).

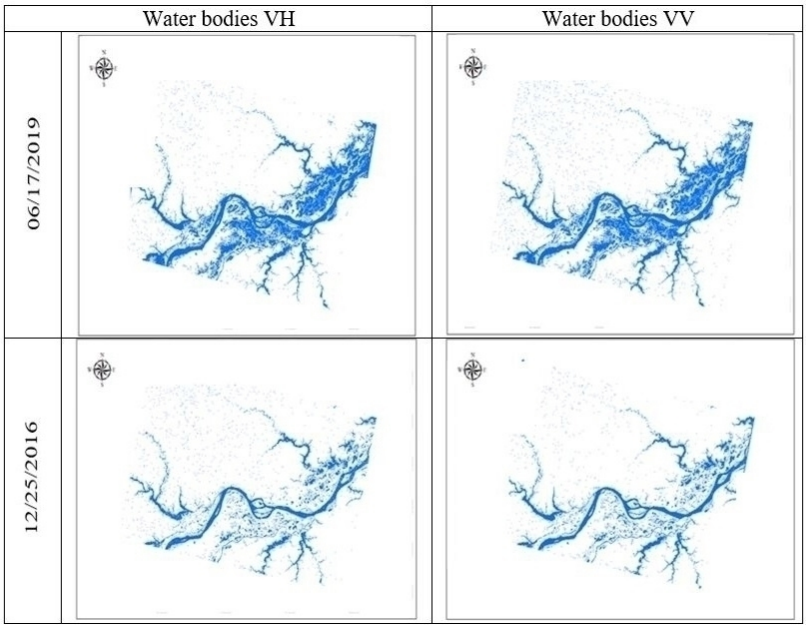

Figure 9 - Map of water bodies in Central Amazonia in periods of lowest and highest flooded area for the years 2016 to 2020 in Sentinel-1's VH and VV polarizations.

The flood pulse in the Central Amazon region occurs with a delay period between 3 to 4 months after the highest rainfall in March. According to Papa et al. (2010), the flood pulse in the Lower Amazon occurs with a delay of four to six weeks to the peak of precipitation in the basin due to its large dimension and hydraulic complexity. According to Arnesen (2012), the flood pulse originates from precipitation at the sources of the Amazon River, when air masses meet the Andes Mountains and gain magnitude downstream of the hydrographic basin, generating tropical rainfall.

Figure 10 represents the water seasonality of the Amazon River, lakes, and its tributaries between 2016 and 2017 through SAR images in the VH and VV polarizations. The first temporal image of January presents the smallest volume of water bodies, showing the continuity of the Amazon River and lakes in periods of drought. The second image from April represents a transition period; after 4 months, there is a significant change in the volume of water bodies, where lower altitude areas, floodplains, and tributaries flood. In the third image, the maximum flood pulse occurs in June, overflowing the water bodies across the plain. The most extensive floodplains remain with practically the same volume for 3 months (June, July, and August). The flooded area remains until mid-September, when the volume of water decreases until reaching the lowest flooded area at the beginning of December, as shown in the fourth image.

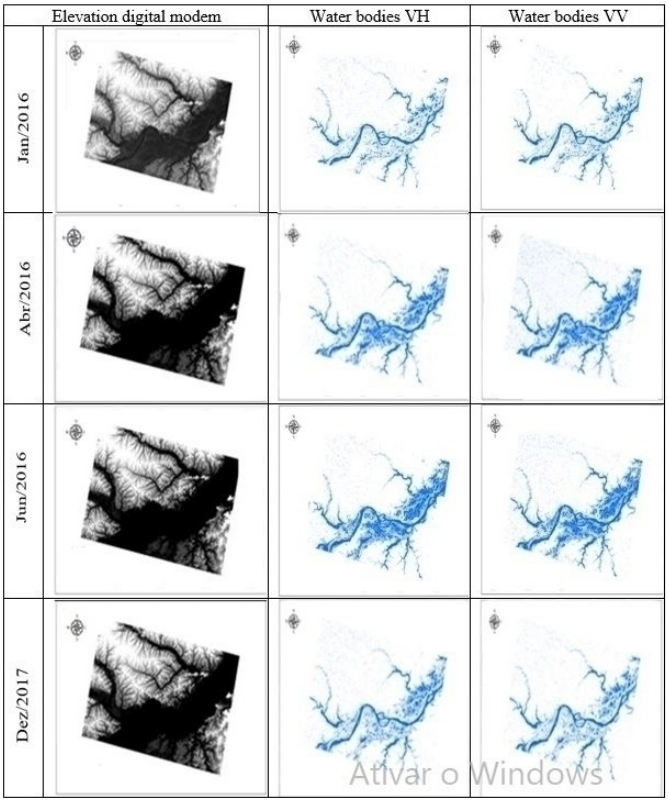

Figure 10 - Seasonal map of the flood pulse in the Amazon River and its tributaries, in January 2016, April, June and December 2017.

The minimum elevation in the fluviometric ruler was 43 cm referring to the image of 11/02/2017, and the maximum height was 902 cm in the image of 06/17/2019. However, the general average was 551 cm, proving the regional perpetuity and considerable volume of water (Table 5.1 and 5.2).

Image date	Quota in station (cm)	Flooded area km² (VH)	Flooded area km² (VV)	Difference km² (VH - VV)
26/09/2016	199	3.212,59	3.910,69	698,10
02/10/2016	170	4.129,09	3.422,44	306,56
14/10/2016	87	3.592,33	3.112,97	479,36
07/11/2016	78	3.701,88	3.266,90	434,98
19/11/2016	79	2.664,99	3.235,6	570,61
13/12/2016	47	3.401,88	3.000,81	401,07
25/12/2016	106	3.059,75	2.868,59	191,16
06/01/2017	260	3.197,43	3.359,09	361,69
30/01/2017	480	3.775,88	3.342,51	433,37
11/02/2017	576	4.225,88	3.759,72	466,16
19/03/2017	748	5.268,08	4.543,67	724,41
31/03/2017	788	5.066,78	4.678,20	388,58
12/04/2017	824	5.401,88	4.874,62	527,26
24/04/2017	850	5.896,42	5.824,30	72,12
18/05/2017	882	5.705,13	5.823,14	35,71
30/05/2017	869	6.103,67	5.861,76	251,91
11/06/2017	859	5.614,82	5.791,11	176,29
23/06/2017	833	6.106,08	6.070,37	118,01
05/07/2017	813	5.683,88	5.433,12	250,76
17/07/2017	780	5.307,53	5.960,31	652,78
10/08/2017	683	5.087,18	5.866,05	778,87
22/08/2017	602	5.311,51	5.791,85	480,34
03/09/2017	467	4.952,00	4.701,58	250,42
15/09/2017	290	4.692,09	5.077,95	385,86
09/10/2017	58	4.168,87	3.599,52	569,35
02/11/2017	43	3.891,61	3.300,61	591
14/11/2017	88	3.463,89	4.276,77	812,88
08/12/2017	175	3.601,09	3.425,46	175,63
20/12/2017	202	3.310,32	3.069,68	240,64

Table 5.1 - Flooded area (km²) through the time series of Sentinel 1-SAR images in VH and VV polarizations.

The smallest elevation value recorded on the ruler did not represent the smallest flooded area in the SAR image; in contrast, the highest elevation value corresponded to the highest inundation area.

Image date	Quota in station (cm)	Flooded area km² (VH)	Flooded area km² (VV)	Difference km² (VH - VV)
01/01/2018	267	3.655,50	3.220,09	435,41
13/01/2018	349	3.794,80	3.618,55	176,25
25/01/2018	411	3.773,86	3.221,76	552,1
06/02/2018	481	3.861,34	3.881,44	20,1
18/02/2018	551	3.837,37	3.481,74	355,63
02/03/2018	605	4.792,88	3.943,44	849,44
14/03/2018	629	4.588,23	4.001,19	587,04
26/03/2018	636	4.649,36	4.359,04	290,32
07/04/2018	663	5.104,47	4.414,60	689,87
19/04/2018	703	4.836,75	4.815,49	21,26
01/05/2018	743	5.246,10	5.051,08	195,02
13/05/2018	790	5.387,74	5.216,44	171,3
12/07/2018	862	5.193,88	5.291,67	97,79
17/08/2018	738	5.095,88	5.010,89	84,99
22/09/2018	379	4.601,88	4.801,89	200,01
16/10/2018	105	4.201,88	4.078,88	123
21/11/2018	82	3.801,64	3.548,88	252,76
15/12/2018	154	3.401,54	3.779,66	378,12
08/01/2019	353	3.849,88	3.755,65	56
01/02/2019	536	3543,13	3.771,54	228,41
09/03/2019	693	4.721,21	4.603,88	118
14/04/2019	760	5.201,78	5.287,76	85,98
08/05/2019	894	6.553,21	6.414,89	138,31
17/06/2019	902	6.611,86	6.443,19	158,67
07/07/2019	818	5.801,46	5.956,53	155,07
12/08/2019	674	5.331,24	5.655.79	324,55
29/09/2019	333	4.507,06	4.235,17	271,89
11/10/2019	105	4.203,9	4.101,9	102
16/11/2019	83	3.375,55	3.575,45	199,9
10/12/2019	137	3.424,12	3.260,83	163,29
15/01/2020	341	3.526,74	3.762,71	235,97
08/02/2020	536	3.902,81	3.813,67	89,14

Table 5.1 - Flooded area (km²) through the time series of Sentinel 1-SAR images in VH and VV polarizations.

Some months showed a sudden increase or decrease in the value of the ruler's quota, but little change occurred in the flooded area, inferring that the extent of the floods is not only related to the Amazon River but also to its tributaries. The measured values of the flooded area through the VH and VV polarizations showed approximate temporal patterns of the water, and the smallest differences happened during the flooding periods.

In the historical series, the VH polarization images obtained the largest flooded areas in the flood period. Clement et al. (2018), when analyzing 13 Sentinel–1 scenes in the Yorkshire region, UK, also obtained larger floodable areas with VH polarization. According to Frota (2019), the Rio Negro flooded area using Sentinel-1 images in the VH polarization (2016 to 2017) overestimated the values.

In general, the two polarizations presented results compatible with the water pattern, being a potential for the definition of flooded areas. Likewise, Hess et al. (2015) analyzed the flood dynamics and obtained good results in distinguishing wetlands through temporal SAR images.

In general, the two polarizations presented results compatible with the water pattern, being a potential for the definition of flooded areas. Likewise, Hess et al. (2015) analyzed the flood dynamics and obtained good results in distinguishing wetlands through temporal SAR images.

STATISTICAL ANALYSIS OF THE FLOODED AREAS

The correlation between the wetlands obtained by the SAR images in the VH and VV polarizations for the studied period obtained an R of 0.89 (figure 11). In the dry period, areas with water ranging from 2 to 3 km² showed more significant divergence between the two polarizations. Wetlands

above 6 km² present greater similarity, positioned close to a straight line. The student's t-test indicated normality between independent samples, confirming the hypothesis of statistical similarity with a t value of 0.70 and a two-tailed critical t of 1.99.

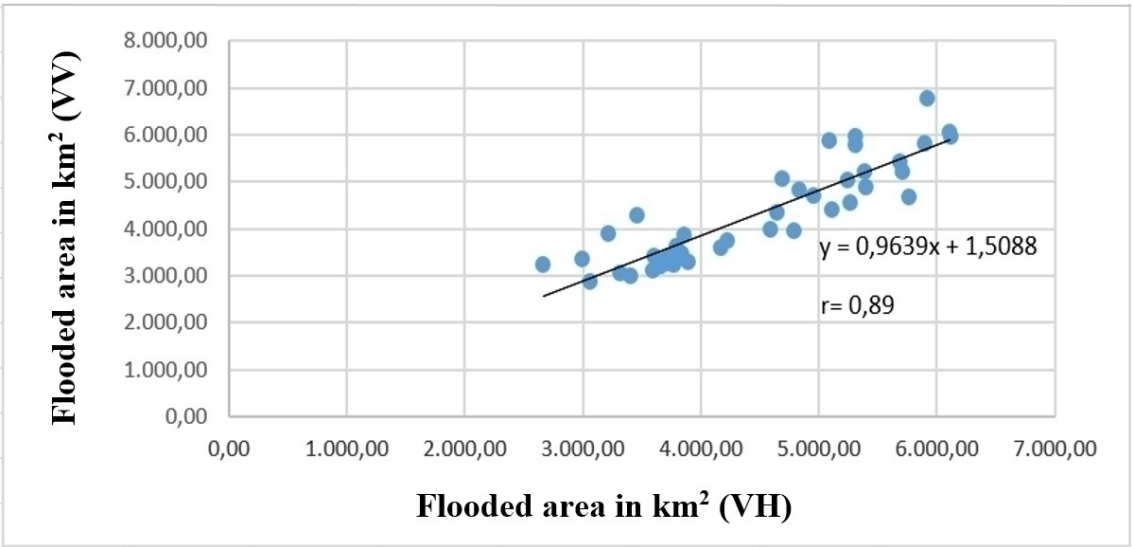

Figure 11 - Linear regression between the flooded areas between the VH and VV polarizations.

Figure 12 shows the regression between the water level in the Parintins (AM) ruler and the flooded areas obtained by the images of the two polarizations. The regression lines of both models are similar, obtaining an R^2 of 0.79 for the VH image and an R^2 of 0.64 for the VV image. Barbosa et al. (2006) used regression models to estimate the flooded areas through the height of the fluviometric ruler, bathymetry and Landsat TM images in the floodplain of Lago de Grande Curaí (AM), obtaining an R^2 of 0.99. This value is higher than that obtained in this study, probably due to the greater number of variables used in the model.

The regression between the relative values of the fluviometric ruler and the flooded areas showed the following characteristics: (a) the most remarkable absolute differences occurred with ruler heights between 400 cm and 600 cm; (b) the flood areas in the VV polarization fit best between the ruler heights from 0 to 200 cm; (c) the flood areas in the VH polarization best fit between the heights of the rulers from 600 to 1000 cm.

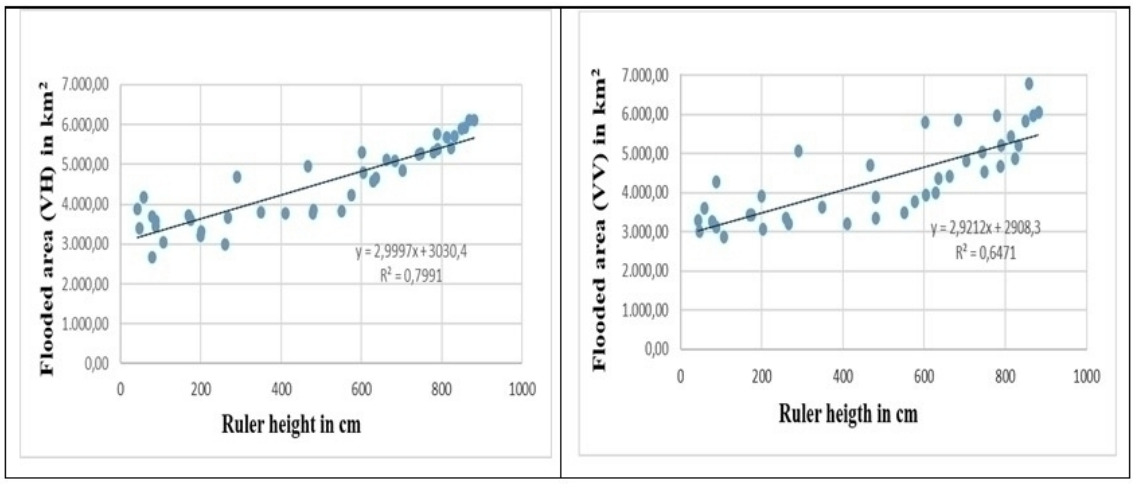

Figure 12 - Linear regression model related to the flooded area in the VH and VV polarizations with the ruler's elevation in Parintins, AM.

ANALYSIS OF "AVERAGE ORDINARY FLOOD LINE

The relative value of the ALOF observed in the fluviometric ruler was 927.36 cm. The events of heavy rains and floods predominated between 1970 and 1988, with several events with values greater than 927.36 cm. The highest measured value was 1,079 cm on June 1, 1971. Between July 2014 and July 2020 (6 years), the relative heights had the lowest values, consistently below 927.36 cm and with a sudden drop in June 2016 (Figure 13).

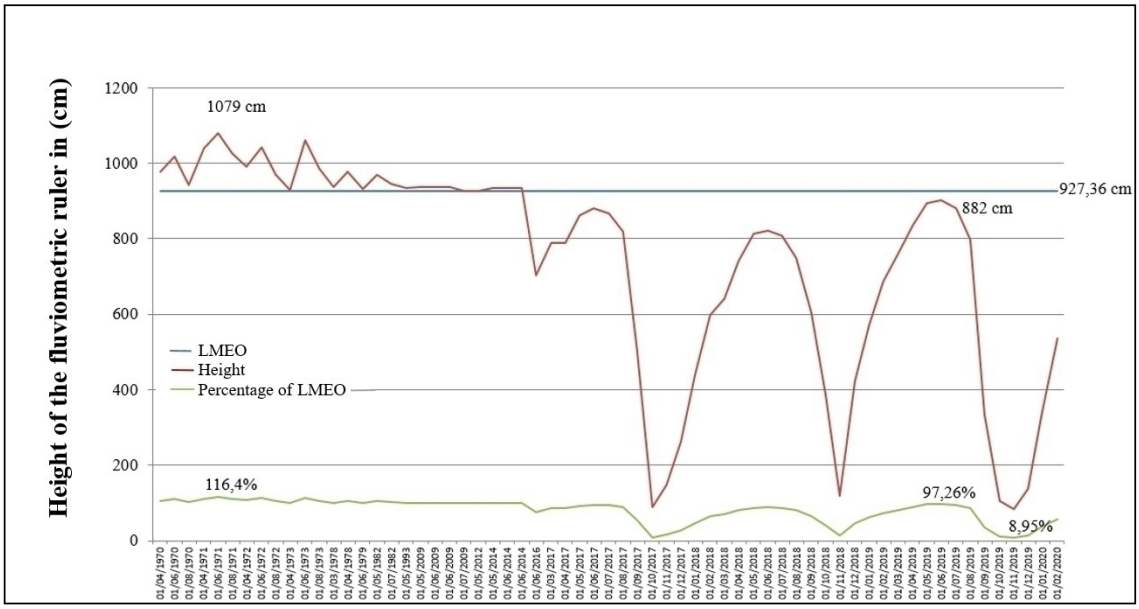

Figure 13 - Graph of the fluviometric regime in the Amazon River between 1967 and 2020 and the relative value of the ALOF.

During the Sentinel-1 time series, the lowest relative height in the fluviometric ruler was 83 cm in November 2019 (Figure 14), and the highest value was 902 cm, reached on June 26, 2019 (Figure 15). Comparing the two periods demonstrates the significant expansion of the water volume in the Amazon River, tributaries, and neighboring lakes in the flood period. The extension of the floodplain showed different dynamics in the period of greater water volume, with a maximum width of 30.48 km on the left bank and 47.74 km on the right bank of the Amazon River.

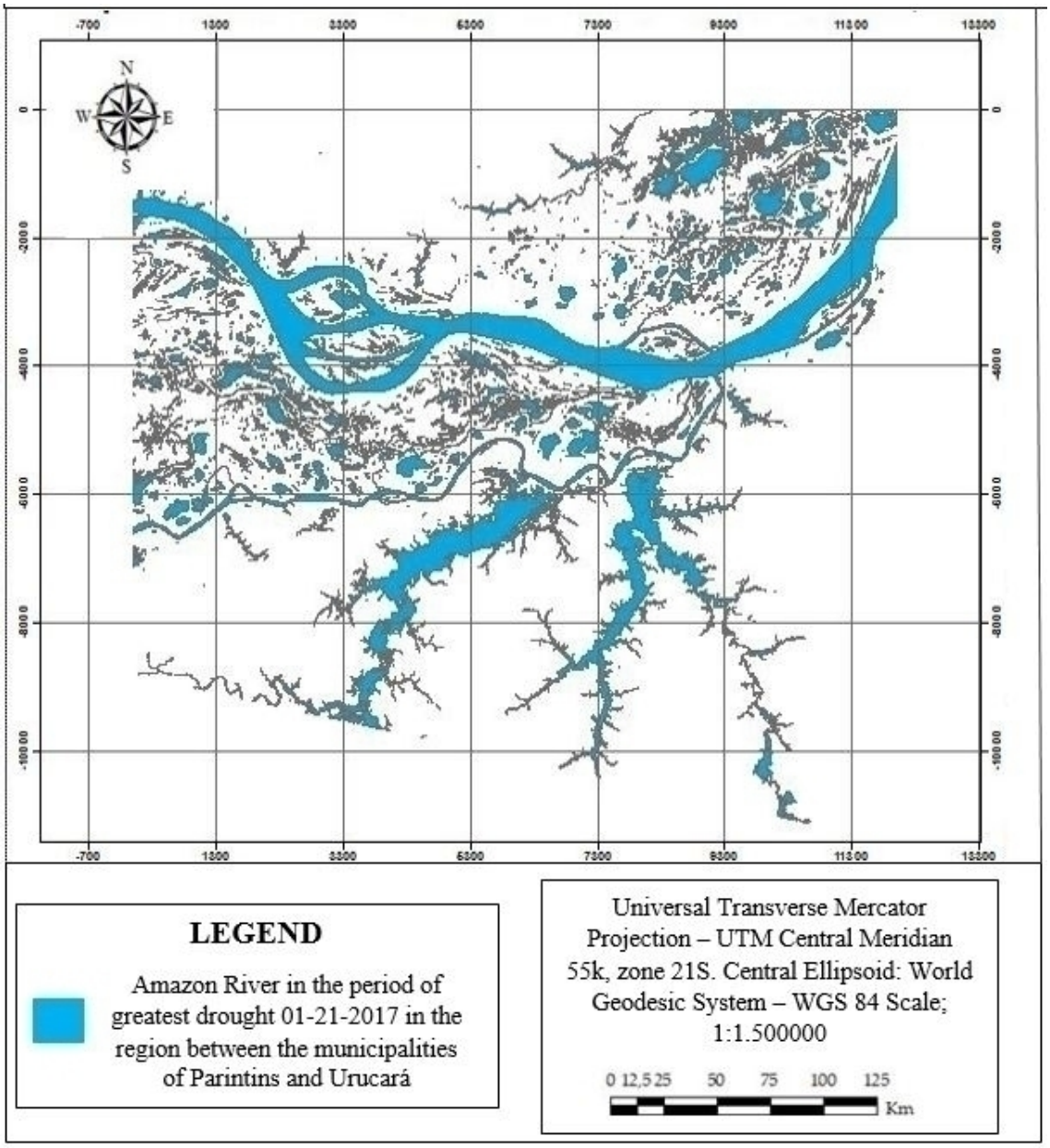

Figure 14 – Map of the flooded areas in a stretch of the Amazon River between the municipalities of Urucara and Parintins in central Amazonia in the period of greatest drought recorded through the time series of Sentinel – 1 SAR images.

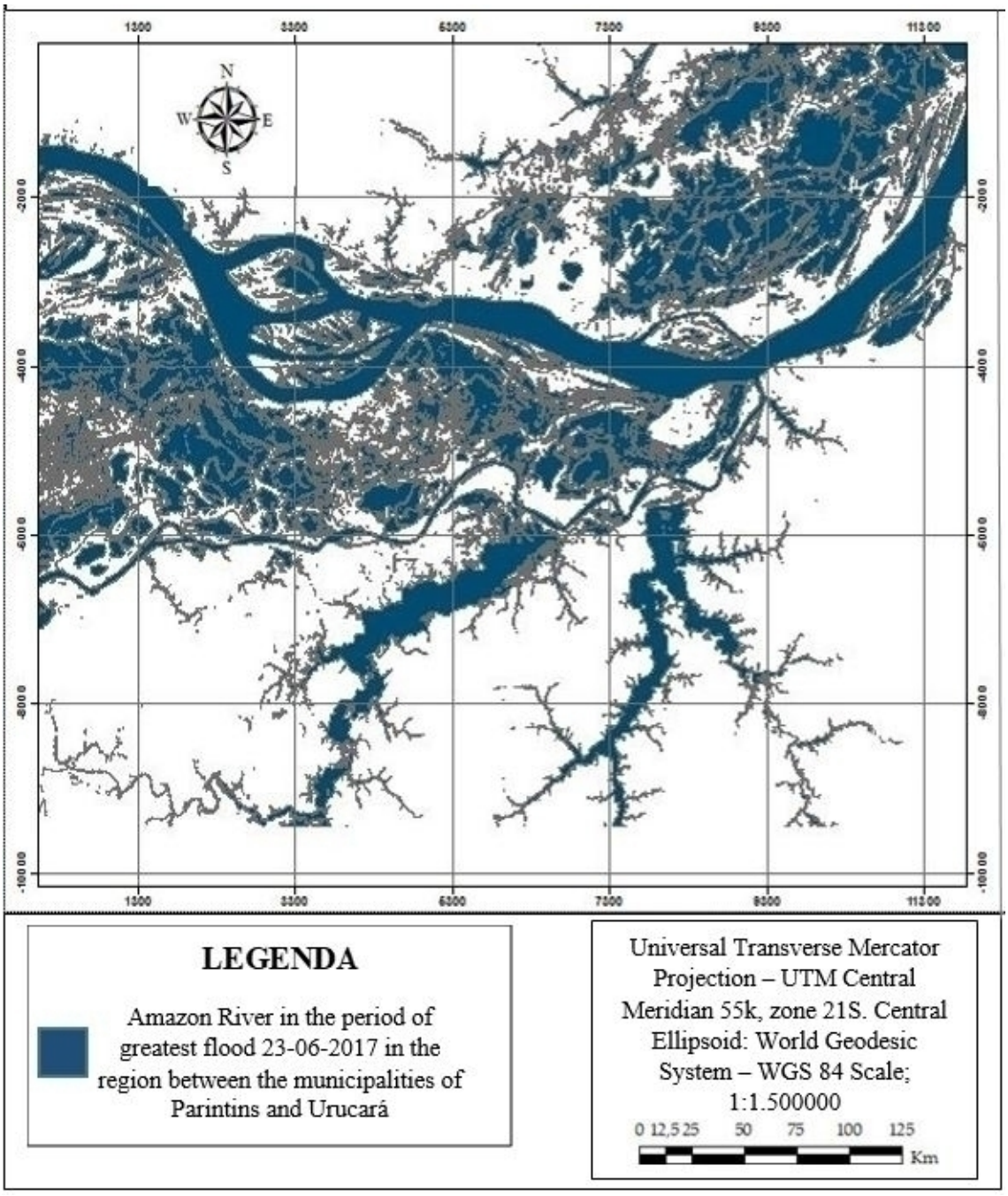

Figure 15 - Map of flooded areas in a stretch of the Amazon River between the municipalities of Urucara and Parintins in central Amazonia in the period of greatest flooding recorded through the time series of Sentinel images – 1 SAR.

CONCLUSION

This study innovates by presenting a methodological approach for mapping flooded areas correlated with data from meteorological stations, as it proved to be effective in mapping floodable areas using remote sensing techniques in time series of SAR Sentinel -1 images. The lack of Sentinel–1 SAR images before 2016, when flood events were greater than ALOF (927.36 cm), made it impossible to delimit the ALOF flood area using SAR data. The linear regression models obtained through the VH and VV polarizations showed satisfactory results. However, the wetlands obtained by the VH polarization images showed a more significant correlation with the fluviometric elevation (79%) than the VV

polarization images (64%). The flood areas measured in the VH and VV polarizations showed good correlation and no statistical significance between the samples, assuming that both polarizations can be used to obtain water volume, dynamics, and delimitation of floodable areas in the region.

REFERENCES

ALMEIDA, F. C. Simulação de Resposta de Estruturas Simplificadas de Vegetação ao Radar de Abertura Sintética Interferométrico. Dissertação (Mestrado). São José dos Campos: Instituto Nacional de Pesquisas Espaciais – INPE, 2008.

BARBOSA, C. C. F.; NOVO, E. M. L. M.; MELACK, J. M.; FREITAS, R. M.; FILHO, W. P. Metodologia de análise da dinâmica de área e volume inundável: o exemplo da Várzea do Lago Grande de Curuai. Revista Brasileira de Cartografia, v. 1, p. 03-24, 2006.

BRASIL. Constituição da República Federativa do Brasil. Brasília, DF, 1998.

CARVALHO JÚNIOR, O. A.; SAMPAIO, C. S.; SILVA, N. C.; COUTO JÚNIOR. A. F.; GOMES, R. A. T.; CARVALHO, A. P. F.; SHIMABUKURO, Y. E. Classificação de Padrões de Savana usando assinaturas temporais NDVI do Sensor MODIS no Parque Nacional Chapada dos Veadeiros. Revista Brasileira de Geofísica, v. 26, n. 4, p. 505-507, 2008.

CHANG, J.; HANSEN, M. C.; PITTMAN, K.; CARROLL, M.; DIMICELI, C. Corn and soybean mapping in the united states using MODN time-series data sets. Agronomy Journal, v. 99, n. 6, p. 1654-1664. 2007.

CLEMENT, M. A.; KILSBY, C. G.; MOORE, P. Multi-temporal synthetic aperture radar flood mapping using change detection. Journal of Flood Risk Management, v. 11, p. 152-168, 2018.

DALLEMAND, J. F.; LICHTENEGGER, J.; RANEY, R. K.; SCHUMANN, R. Radar Imagery. Theory and Interpretation (Lecture Notes). Roma: FAO, 118 p. 1993.

DONG, Y. M.; MILNE, A. K.; FORSTER, B.; C. Segmentation and Classification of Vegetated Areas Using Polarimetric SAR Image Data. IEEE Transactions on Geoscience and Remote Sensing, v. 39, n. 2, p. 321-329, 2001.

EUROPEAN SPACE AGENCY - ESA. Disponível em:

< https://sentinel.esa.int/web/sentinel/home>. Acesso em: 07 de Jan. 2019.

FERREIRA, G. H. S. Identificação de áreas inundáveis na porção sul de Roraima com auxílio de imagens de Radar. Dissertação (Mestrado). Brasília: Universidade de Brasília - UNB, 2018.

FORKUOR, G.; CORAND, C.; THIEL, M.; ULMANN, T.; ZOUNGRANA, E. Integration of Optical and Synthetic Aperture Radar Imagery for Improving Crop Mapping in Northwestern Benin, West Africa. Remote Sensing, v. 6, n. 7, p. 6472-6499, 2014.

FROTA, S. M. N. Relação entre área de inundação e cota fluviométrica na sub-bacia do Alto rio Negro: uma análise baseada em dados de radar (Sentinel-1A). Dissertação (Mestrado). Brasília: Universidade de Brasília - UNB, 2019.

FURTADO, L. F. A.; SILVA, T. S. F.; NOVO, E. M. L. M. Dual-season and full-polarimetric C band SAR assessment for vegetation mapping in the Amazon várzea wetlands. Remote Sensing of Environment, v. 174, p. 212-222, 2016.

GARDIMAN JUNIOR. B. S; MAGALHÃES, I. A. L; FREITAS, C. A. A; CECÍLIO, R. A. Análise de técnicas de interpolação para espacialização da fusão pluvial na bacia do rio Itapemirim (ES). Ambiência, v. 8, n.1, p. 61–71, 2012.

HESS, L. L.; MELACK, J. M.; AFFONSO, A. G.; BARBOSA, C.; GASTIL-BUHL, M.; NOVO, E. M. L. M. Wetlands of the Lowland Amazon Basin: Extent, Vegetative Cover, and Dual-season Inundated Area as Mapped with JERS-1 Synthetic Aperture Radar. Wetlands, v. 35, p. 745-756, 2015.

INSTITUTO NACIONAL DE METEOROLOGIA - INMET. BDMEP - Banco de Dados Meteorológicos para Ensino e Pesquisa. Disponível em: http://www.inmet.gov.br/portal/index.php?r=bdmep/bdmep. Acesso em: 25 abr. 2020.

JUNK, W. J. The Central Amazon Floodplain - Ecology of a Pulsing System. New York: Springer, 1997. 525p.

LEE, J. S. Digital image enhancement and noise filtering by use of local statistics. IEEE Trans. Pattern Analysis and Machine Intelligence, v. 2, n. 2, p. 165-168, 1980.

LEE, J. S.; POTTIER, E. Polarimetric SAR Radar Imaging: From Basic to Applications. Boca Raton: CRC Press, 2009. 422p.

MANSOURPOUR, M.; RAJABI, M. A; BLAIS, J. A. R. Effects and performance of speckle noise reduction filters on active radar and SAR images. ISPRS Journal of Photogrammetry & Remote Sensing, v. 1, p. 1-9 2006.

MARINHO, R. R.; PARADELLA, W. R.; RENNO, C. D.; OLIVEIRA, C. G. Aplicação de imagens SAR orbitais em desastres naturais: Mapeamento das inundações de 2008 no Vale do Itajaí, SC. Revista Brasileira de Cartografia, v. 64, p. 317-330, 2012.

MARQUES, J. B. Uso de Série temporal de imagens PALSAR-2/ALOS 2 para classificação de uso e cobertura do solo e detecção de áreas úmidas na região da Ilha do Bananal, trecho médio do Rio Araguaia. Dissertação (Mestrado). Brasília: Universidade de Brasília - UNB, 2017.

MELACK, J. M.; HESS, L. L. Remote Sensing of the Distribution and Extent of Wetlands in the Amazon Basin. Amazonian Floodplain Forests. Ecological Studies (Analysis and Synthesis). Dordrecht Springer, v. 210, p. 43-59, 2010.

PAPA, F.; PRIGENT, C.; AIRES, F.; JIMENEZ, C.; ROSSOW, W. B.; MATTHEWS, E. Interannual variability of surface water extent at global scale. Journal of Geophyical Research, v. 115, n. 112, p. 1-17, 2010.

SANTOSO, A. W.; BAYUAJI, L.; TIEN SZE. L.; LATEH, H.; ZAI, J. M. Comparison of Various Speckle Noise Reduction Filters on Synthetic Aperture Radar Image. International Journal of Applied Engineering Research, v. 11, p. 8760-8767, 2016.

RAMALHO, E. E.; MACEDO, J.; VIEIRA, T. M.; VALSECCHI, J.; CALVIMONTES, J.; MARMONTEL, M.; QUEIROZ, H. L. Ciclo hidrológico nos ambientes de várzea da reserva de desenvolvimento sustentável Mamirauá – Médio rio Solimões, período de 1990 A 2008. UAKARI, v. 5, n.1, p. 61-87, 2009.

SECRETARIA DO PATRIMÔNIO DA UNIÃO - SPU. Orientação Normativa que disciplina a demarcação de terrenos marginais e seus acrescidos (ON-GEADE-03). Relatório, 2001. Disponível em: . Acesso em: jun. 2018.

TELLO, M.; LOPEZ-MARTINEZ, C.; MALLORQUI, J. J. Automatic vessel monitoring with single and multidimensional SAR images in the wavelet domain. ISPRS Journal of Photogrammetry & Remote Sensing, v. 61, p. 260-278, 2006.